applied optics

Basic geometry and aberration characteristics of conicoidal conformal domes

Fanyang Dang,[1] Wang Zhang,[1] Shouqian Chen,[1] Hui Wang,[1] Van Nhu Le,[2] Jiaqian Yu,[1] and Zhigang Fan[1,*]

[1]Research Center of Space Optical Engineering, Harbin Institute of Technology, Heilongjiang, Harbin 150001, China
[2]Le Quy Don Technical University, 236 Hoang Quoc Viet Street, Hanoi, Vietnam
*Corresponding author: fzg@hit.edu.cn

Received 16 June 2016; revised 10 August 2016; accepted 5 September 2016; posted 23 September 2016 (Doc. ID 268252); published 24 October 2016

This paper investigated the geometry and aberration characteristics of conicoidal conformal domes. First, on the basis of previous research, we got the expression that was suitable for describing the external surface of the conicoidal conformal dome. Based on the theory of differential geometry, this paper first proved that the Dupin index line of a quadric surface was an ellipsoid and the radius of curvature had extreme values in the meridian plane and sagittal plane. Then the uniform formulas of curvature which were suitable for ellipsoid, paraboloid, and hyperboloid were deduced in the meridian plane and sagittal plane, respectively. Meanwhile, the angle between the axis of imaging systems and the surface normal was calculated. With the help of computers, the plots of curvature differences and the angle in the case of different edge slopes, fineness ratios, and the locations of the rotational center were obtained. Finally, we analyzed the Zernike polynomial coefficients of Z4, Z5, and Z8, which represent defocus, astigmatism and coma, respectively for the model established in CODE V. The research indicates that the dynamic ranges of defocus, astigmatism, and coma increase with the growing of edge slopes and fineness ratios, but have little change with the variation of the rotational center positions. Moreover, the curves of Z5 and Z8 have turning points, and the curves of curvature differences and angle difference are only similar to the curves of Z5 and Z8 when the look angle changes after the turning point. For the look angle changing from zero to the turning point, the curves of Z5 and Z8 change rapidly. This is mainly caused by the significant variations of the symmetry of the conformal dome participating in imaging. Therefore, the aberrations with small scanning angles should be given more attention when designing the conformal systems.

OCIS codes: (080.1005) Aberration expansions; (080.2468) First-order optics.

http://dx.doi.org/10.1364/AO.55.008713

1. INTRODUCTION

Missiles with infrared guided seekers have lots of advantages: high resolution, long observation distance, and strong anti-interference ability, etc. Generally, infrared guided seekers work in the scanning mode, and the imaging system rotates around a fixed point, which is called the rotational center. Traditional optical domes have been a section of concentric spheres or hemispheres. Although the domes have good imaging quality, they produce large air drag [1]. Therefore, in order to reduce air drag and improve missile performance, conformal optical technology is developed. Conformal domes are characterized as having external surfaces that are first optimized for aerodynamics requirements rather than optical systems. They typically take the form of an ogive dome and blend smoothly with missiles. The missile with a conformal dome can fly farther and faster than that with a traditional dome [2,3]. In addition, conformal domes make a great contribution to expand the field of regard (FOR). However, the improved performance comes with some design challenges. Because of losing point symmetry, different parts of the conformal dome participate in imaging with a different look angle. This introduces lots of dynamic aberrations into the system [4,5]. The dynamic aberrations mainly include spherical aberration, coma, and astigmatism [6]. Therefore, analyzing the characteristic of these aberrations is very important to correct them.

The research of conformal technology mainly includes the aero-optic and aerothermal analysis or the technologies of correcting aberrations [4,7]. The methods of correcting aberrations are the fixed corrector, the arch corrector, the counter-rotating phase plates, and the deformable mirror, etc. [4,5]. These correctors generally use complex surfaces, which include quadric surfaces, aspheric surfaces, or freeform surfaces. The freeform surfaces may be expressed by Zernike

polynomials, XY-polynomials, or NURBS surfaces, etc [8,9]. In short, comparing with traditional optical systems, the conformal optical systems have great difficulty in design and manufacture [10,11]. Meanwhile, the conformal dome itself also has the problem of design and manufacture. From the research papers of conformal domes, we know the conformal domes primarily are conicoidal conformal domes. But the research mainly focuses on ellipsoidal domes or paraboloidal domes, respectively, and lack system analysis between them. Therefore, based on the mathematical descriptions of conicoidal conformal domes studied by previous researchers [6], this paper will study the basic geometry and aberration characteristics of conicoidal conformal domes systematically.

The research contents include: (1) investigate the uniform formulas suitable for quadric surfaces, which include the radius of curvature and the angle between the axis of imaging systems and the surface normal, then calculate the radius of curvature and the angle with different geometric parameters; (2) establish the model of conicoidal conformal domes in optical design software CODE V and research the Zernike aberrations under different conditions; (3) compare the geometric property of the quadric surface with the Zernike aberrations of the conicoidal conformal dome, then research the relations between them.

2. MATHEMATICAL DESCRIPTIONS OF CONICOIDAL CONFORMAL DOMES

The optical dome has two surfaces: the external one and the inner one. Generally, the external surface decides the type of the optical dome, and the inner surface is used to correct aberrations [10]. The length L and the diameter D are the key parameters to determine the shape and function of the dome. As shown in Fig. 1, o' is the rotational center of the imaging system. The fineness ratio F is defined as the ratio of L to D, which primarily determines the aerodynamic drag. Generally, the aerodynamic drag would reduce with the increasing of the fineness ratio F.

For a conicoidal conformal dome, the external surface is a quadric surface. There are several descriptions of a quadric surface, and Fig. 2 is one of them. The vertex of the quadric surface is located in the origin of the Cartesian coordinate system and the z-axis is the symmetry axis.

Point P is located on the external surface of the conicoidal conformal dome. The distance from point P to the z-axis can be expressed by the following equation:

$$\varphi(z) = [2Rz - (k+1)z^2]^{1/2}. \tag{1}$$

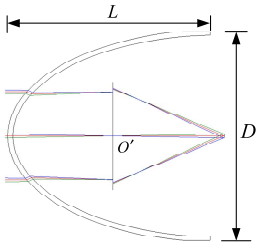

Fig. 1. Schematic diagram of a conformal optical dome.

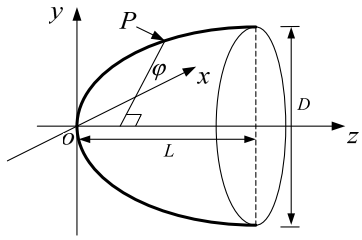

Fig. 2. Model of a conicoidal conformal dome.

In Eq. (1), R is the radius of curvature of the vertex (or called the base circle radius) and k is the conic constant. In order to calculate the value of R and k, we subsequently differentiated Eq. (1) and got the expressions of R and k as the following [6]:

$$k = \frac{\varphi^2}{z^2} - \frac{2\varphi}{z}\varphi' - 1, \tag{2}$$

$$R = \varphi\varphi' + (k+1)z, \tag{3}$$

where $\varphi' = d\varphi/dz$.

Because Eqs. (2) and (3) are valid for every point on the surface, we take the point on the bottom edge and substitute φ, z by the dome shape specifications ($\varphi \to D/2$, $z \to L$) in Eqs. (2) and (3), then rewrite the expressions of R and k as follows:

$$k = \frac{D^2}{4L^2} - \frac{D}{L}S_e - 1, \tag{4}$$

$$R = \frac{D^2 + 4L^2(k+1)}{8L}, \tag{5}$$

where $S_e = \varphi'|_{z=L}$ is the edge slope.

Defining q as the slope coefficient and making $S_e = D/qL$, then Eqs. (2) and (3) become

$$k = \frac{(q-4)D^2}{4qL^2} - 1, \tag{6}$$

$$R = \frac{(q-2)D^2}{4qL}. \tag{7}$$

For an ellipsoidal dome, $-1 < k < 0$, so $q > 4$; when $q = 4$, $k = -1$, the surface is a paraboloid. But if $q = 2$, it becomes a conic surface, so for a hyperboloid, $2 < q < 4$. The formulas of base circle radius and conic constant of conicoidal conformal domes changing with slope coefficient q or edge slope S_e are shown in Table 1. It can be seen from Table 1 that if the length L and the bottom diameter D are determinate, the edge slope S_e will decide the surface type. When $S_e = 0$, the surface is an ellipsoid, then it changes to a paraboloid with

Table 1. Base Circle Radius and Conic Constant of a Quadric Surface

Surface Type	q	S_e	Conic Constant (k)	Base Circle Radius (R)
Ellipsoid	$q > 4$	$\frac{D}{qL}$	$\frac{(q-4)D^2}{4qL^2} - 1$	$\frac{(q-2)D^2}{4qL}$
Paraboloid	$q = 4$	$\frac{D}{qL}$	-1	$\frac{D^2}{8L}$
Hyperboloid	$2 < q < 4$	$\frac{D}{qL}$	$\frac{(q-4)D^2}{4qL^2} - 1$	$\frac{(q-2)D^2}{4qL}$

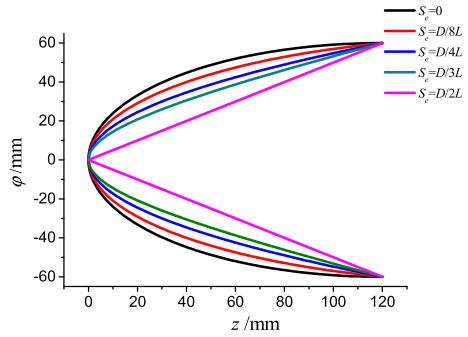

Fig. 3. Geometric graph of $S_e = 0$, $S_e = D/8L$, $S_e = D/4L$, $S_e = D/3L$, $S_e = D/2L$ ($D = 120$ mm, $L = 120$ mm).

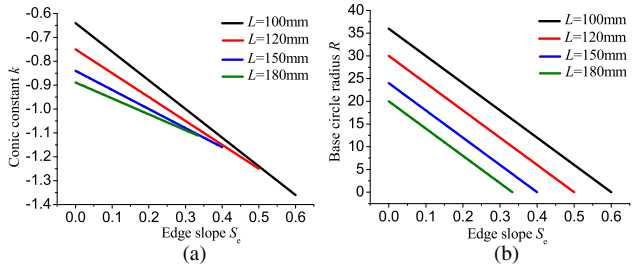

Fig. 4. Conic constant k and base circle radius R changing with the edge slope for different fineness ratios $F(D = 120$ mm).

S_e growing to $D/4L$. Keeping on growing of S_e until $D/2L$, the surface becomes a hyperboloid. Figure 3 is a plot for $S_e = 0$, $S_e = D/8L$, $S_e = D/4L$, $S_e = D/3L$, $S_e = D/2L$ of the dome specifications with $L = 120$ mm and $D = 120$ mm; it shows the dome becomes cuspidal with the increasing of S_e.

Figure 4 is the plot of the conic constant k and base circle radius R changing with the edge slope in different fineness ratios F. The plot indicates that the conic constant k and base circle radius R decrease linearly with the growing of the edge slope S_e, and they have smaller values for the dome with a bigger fineness ratio.

3. GEOMETRIC CHARACTERISTIC OF QUADRIC SURFACES

A. Radius of Curvature of a Quadric Surface

Comparing with spheres, the curvature of quadric surfaces is different in each position. This will produce dynamic aberrations, so we calculate the curvature of quadric surfaces to evaluate the dynamic aberrations. In order to analyze the curvature in different directions at any point along quadric surfaces, we use vector functions expressing spatial curves and spatial surfaces. A spatial surface can be expressed as $\vec{r} = \vec{r}(u, v)$, and the expression of a spatial curve on the spatial surface is $\vec{r} = \vec{r}(u, v) = \vec{r}[u(t), v(t)] = r(t)$, where u, v, and t are free variables. The tangent vector of a spatial curve is the differential of $\vec{r}$, and it can be expressed as $\vec{r}'(t) = \vec{r}_u(du/dt) + \vec{r}_v(dv/dt)$, which indicates $\vec{r}'(t)$, $\vec{r}_u$, $\vec{r}_v$ in the same plane. The plane decided by $\vec{r}_u$ and $\vec{r}_v$ is defined as the tangent plane

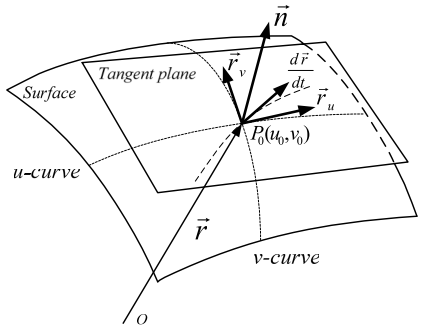

Fig. 5. Schematic diagram of the tangent plane and surface normal.

of the spatial surface at one point on it, as shown in Fig. 5. The vertical vector of the tangent plane is defined as the normal vector of the surface, and the unit normal vector can be expressed as

$$\vec{n} = \frac{\vec{r}_u \times \vec{r}_v}{|\vec{r}_u \times \vec{r}_v|}. \tag{8}$$

For a point P on the surface, the normal section is the plane decided by the tangent vector and the normal vector. The normal section line is defined as the intersecting line between the surface and the normal section. Therefore, the curvature center of the normal section line is located in the normal section. Assuming k_n is the curvature of the normal section line at the point P, the Dupin index line is defined as the track of N in the tangent plane, while the length of PN equals $\sqrt{|1/k_n|}$, as shown in Fig. 6. If we can obtain the equation of the Dupin index line, the curvature of the quadric surface is known.

For a quadric surface, it can be expressed as follows:

$$\vec{r} = \vec{r}(z, \alpha) = \{\varphi(z)\cos\alpha, \varphi(z)\sin\alpha, z\}, \tag{9}$$

where α is the rotation angle relative to the $x - z$ plane.

Through calculating three basic values (L_s, M_s, and N_s), the equation of the Dupin index line can be deduced:

$$L_s = \vec{r}_{zz} \cdot \vec{n} = -\frac{\varphi''}{\sqrt{1 + \varphi'^2}}, \tag{10}$$

$$M_s = \vec{r}_{z\alpha} \cdot \vec{n} = 0, \tag{11}$$

$$N_s = \vec{r}_{\alpha\alpha} \cdot \vec{n} = \frac{\varphi}{\sqrt{1 + \varphi'^2}}. \tag{12}$$

From the theory of differential geometry, the equation of the Dupin index line for the point on a quadric surface is given by

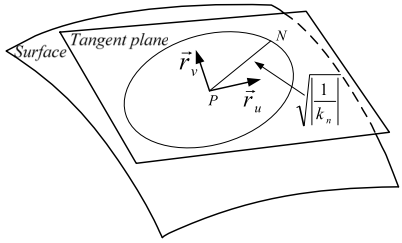

Fig. 6. Definition of the Dupin index line.

$$L_s x_z^2 + 2M_s x_z y_\alpha + N_s y_\alpha^2 = \pm 1, \tag{13}$$

where x_z and y_α satisfy the relation of $\vec{PN} = x_z\vec{r}_z + y_\alpha\vec{r}_\alpha$.

Because of $\varphi > 0$, $\varphi'' = -R^2/\varphi^3 < 0$, so $L_s > 0$, $N_s > 0$. Therefore, the equation of the Dupin index line of a quadric surface is an ellipsoid, as expressed in Eq. (14):

$$-\frac{\varphi''}{\sqrt{1+\varphi'^2}}x_z^2 + \frac{\varphi}{\sqrt{1+\varphi'^2}}y_\alpha^2 = 1. \tag{14}$$

Equation (14) indicates the radius of curvature has extreme values in the direction of $\vec{r}_z$ and $\vec{r}_\alpha$, and the radius of curvature in other orientations varies between them.

Now, we calculate the maximum and minimum radius of curvature of a quadric surface. As the reason of rotational symmetry, we only need to analyze the point on the intersecting line between the surface and the plane crossing the rotational axis. For the point on the $y-z$ plane along the surface, $\vec{r}_z$ and $\vec{r}_\alpha$ are the vectors in the meridian plane and sagittal plane, respectively. Therefore, the radius of curvature has extreme values in the meridian plane and sagittal plane. Setting $y_\alpha = 0$ in Eq. (14), we got $PN = \sqrt{1/k_m} = x_z|\vec{r}_z| = \sqrt{1/L_s}|\vec{r}_z|$. So the radius of curvature in the meridian plane R_m can be expressed as Eq. (15). The z-coordinate z_m and the y-coordinate y_m of the curvature center in the meridian plane are expressed as Eqs. (16) and (17), respectively:

$$R_m = \frac{1}{k_m} = \frac{|\vec{r}_z|^2}{L_s} = -\frac{(1+\varphi'^2)^{3/2}}{\varphi''}, \tag{15}$$

$$z_m = z - \frac{\varphi'(1+\varphi'^2)}{\varphi''}, \tag{16}$$

$$y_m = \varphi + \frac{1+\varphi'^2}{\varphi''}. \tag{17}$$

In the similar way, for the sagittal plane, setting $x_z = 0$, we got $PN = \sqrt{1/k_s} = y_\theta|\vec{r}_\theta| = \sqrt{1/N_s}|\vec{r}_\theta|$. So the radius of curvature in the sagittal plane R_s can be expressed as Eq. (18). The z-coordinate z_s and the y-coordinate y_s of the curvature center in the sagittal plane are expressed as Eqs. (19) and (20), respectively:

$$R_s = \frac{1}{k_s} = \frac{|\vec{r}_\theta|^2}{N_s} = \varphi\sqrt{1+\phi'^2}, \tag{18}$$

$$z_s = z + \varphi\varphi', \tag{19}$$

$$y_s = 0. \tag{20}$$

For a point P in the $y-z$ plane on the surface, using Eqs. (16) and (17), we can get the tracks of curvature centers in the meridian plane for different surface types. Figure 7 is the track of curvature centers in the meridian plane for $S_e = 0$, $S_e = D/8L$, $S_e = D/4L$, and $S_e = D/3L$, respectively, ($D = 120$ mm, $L = 120$ mm). As can be seen from the figures, the curvature centers in the meridian plane keep away from the vertex with the increasing of the edge slope. Equation (20) indicates the curvature centers in the sagittal plane are on the z-axis regardless of the surface type.

Using Eqs. (15) and (18), we can calculate the radius of curvature in the meridian plane and the sagittal plane. It is important to understand the dynamic aberrations. Figure 8 shows the radius of curvature in the meridian plane and the sagittal plane changing with the z-coordinate at different edge slopes when $D = 120$ mm, $L = 120$ mm. As shown in Fig. 8, the meridian radius of curvature is larger than the sagittal radius of curvature obviously. Figure 9 is the plot of the radius of curvature in the meridian plane and the sagittal plane, respectively, at different edge slopes in the same graph. It can be seen from Fig. 9 that the meridian radius of curvature increases with the growing of the edge slope rapidly, while the sagittal radius of curvature has little difference.

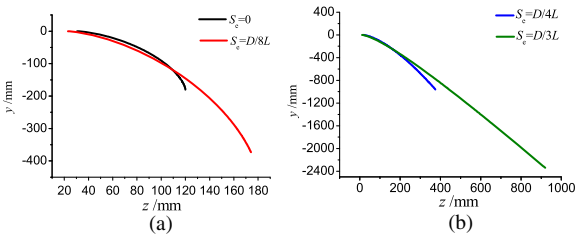

Fig. 7. Track of curvature centers in the meridian plane for $S_e = 0$, $S_e = D/8L$, $S_e = D/4L$, and $S_e = D/3L$ ($D = 120$ mm, $L = 120$ mm).

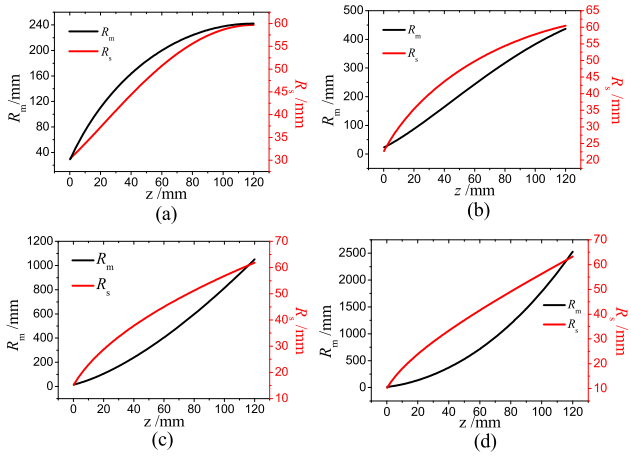

Fig. 8. Radius of curvature in the meridian plane and sagittal plane for (a) $S_e = 0$, (b) $S_e = D/8L$, (c) $S_e = D/4L$, (d) $S_e = D/3L$, ($D = 120$ mm, $L = 120$ mm).

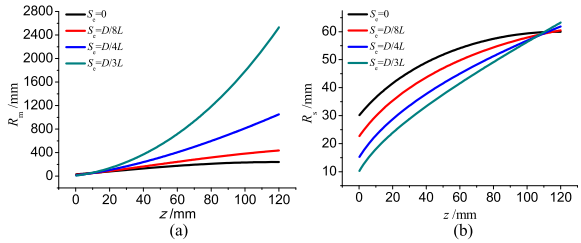

Fig. 9. Radius of curvature in the meridian plane and sagittal plane for $S_e = 0$, $S_e = D/8L$, $S_e = D/4L$, $S_e = D/3L$, ($D = 120$ mm, $L = 120$ mm).

B. Angle Between the Axis of Imaging Systems and the Surface Normal

When imaging systems with conformal domes work in the scanning mode for a seeker, the angle between the axis of the imaging systems and the symmetry axis of the domes is the look angle. Obviously, the maximum look angle is the FOR. Figure 10 is the schematic diagram of a seeker with the conformal dome and working in the scanning mode. In Fig. 10, z_0 is the distance from the dome vertex to the rotational center of the imaging system. θ is the look angle and i_n is the angle between the surface normal and the z-axis. The angle difference between i_n and θ is $\Delta\theta$, which is the angle between the axis of the imaging system and the surface normal.

The expression of angle difference $\Delta\theta$ is given by Eq. (21):

$$\Delta\theta = i_n - \theta = \arctan\frac{1}{\varphi'} - \arctan\frac{\varphi}{z_0 - z}. \tag{21}$$

Assuming $\Delta\theta = 0$, we can get the position of the point that the axis of the imaging system overlaps the surface normal. The z-axis coordinate of the point on the surface is

$$z|_{\Delta\theta=0} = \frac{R - z_0}{k}. \tag{22}$$

From the differential of Eq. (21), we can get the position of the point that the angle difference $\Delta\theta$ has extreme values. The z-axis coordinate of the point satisfies Eq. (23), which is a univariate cubic equation when k and z_0 satisfy $k \neq -1$ and $z_0 \neq R/(k+1)$:

$$az^3 + bz^2 + cz + d = 0. \tag{23}$$

The expressions of coefficients a, b, c, and d are

$$\begin{cases} a = k(k+1)R - k(k+1)^2 z_0 \\ b = -kR^2 + 3k(k+1)Rz_0 \\ c = -R^3 - (3k-1)R^2 z_0 \\ d = R^3 z_0 - R^2 z_0^2 \end{cases}. \tag{24}$$

From Eq. (21), we get the plot of the angle difference $\Delta\theta$ varying with the look angle θ for different edge slope S_e when $D = 120$ mm, $L = 120$ mm, $z_0 = 80$ mm, as shown in Fig. 11. The plot also gives the position of extreme values. It can be seen from Fig. 11 that the surface with a smaller edge slope has a smaller angle difference when the look angle is less than nearly 50°. Meanwhile, the max angle difference increases with the augment of the edge slope, and it appears in lower look angle. Therefore, the dome with a lower edge slope benefits reducing the angle difference for decided length L and diameter D.

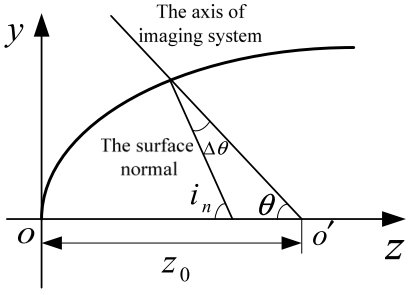

Fig. 10. Schematic diagram of a seeker with the conformal dome working in scanning mode.

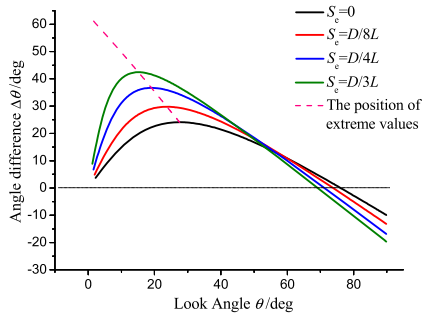

Fig. 11. Angle difference varying with the look angle for different edge slopes when $D = 120$ mm, $L = 120$ mm, $z_0 = 80$ mm.

In the same way, we also get the graph of the angle difference varying with the look angle at different fineness ratios using Eq. (21). As can be seen from Fig. 12, the fineness ratio has an effect on the angle difference varying with the look angle similar to the edge slope. The angle difference increases with the augment of the fineness ratio.

C. Effect of Edge Slopes, Fineness Ratios, and the Position of the Rotational Center of the Imaging System

Comparing with the sphere domes, a seeker with the conformal dome and working in the scanning mode can choose a flexible position of the rotational center of the imaging system. Therefore, the edge slope, fineness ratio, and the position of the rotational center of the imaging system are three factors that may affect the aberrations introduced by the conformal dome except the thickness and refractive index. Based on the earlier research, we study the difference of curvature radius and angle difference in the case of different edge slopes, fineness ratios, and the positions of rotational centers subsequently. Figures 13 and 14 are the plots of the difference of curvature

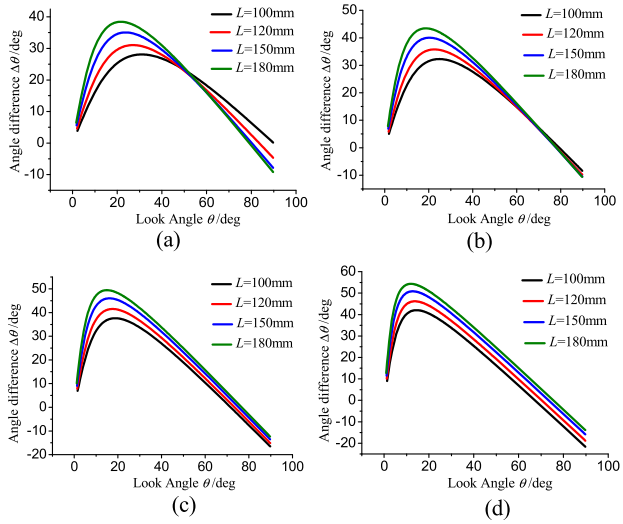

Fig. 12. Angle difference varying with the look angle for different fineness ratios with (a)$S_e = 0$, (b) $S_e = D/8L$, (c) $S_e = D/4L$, (d) $S_e = D/3L$ when $D = 120$ mm, $z_0 = 100$ mm.

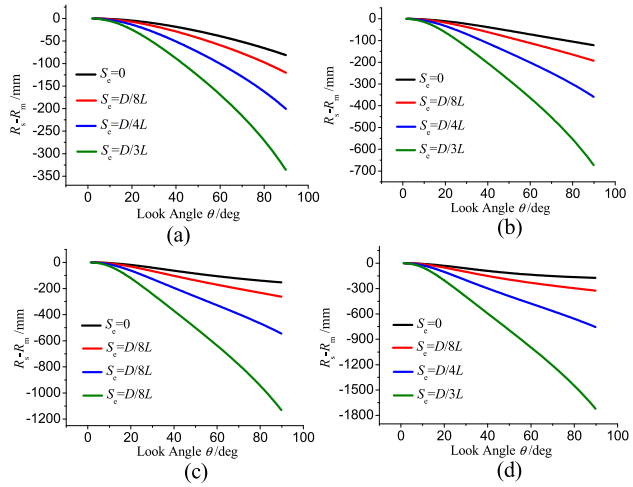

Fig. 13. Difference of curvature radius varying with the look angle for different edge slopes S_e with (a) $z_0 = 40$ mm, (b) $z_0 = 60$ mm, (c) $z_0 = 80$ mm, (d) $z_0 = 100$ mm when $D = 120$ mm, $L = 120$ mm.

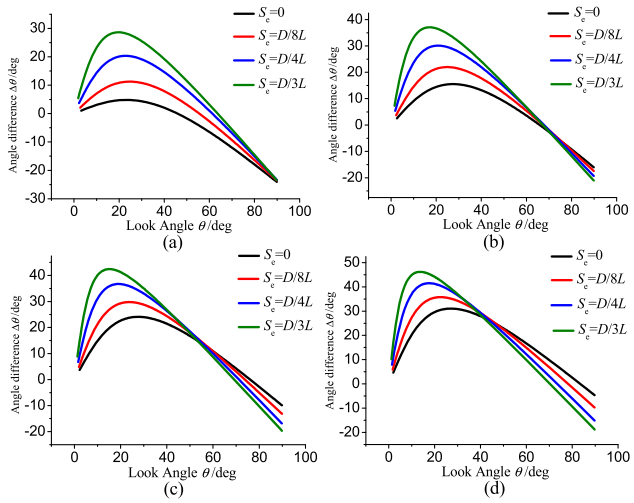

Fig. 15. Angle difference varying with the look angle for different edge slopes S_e with (a) $z_0 = 40$ mm, (b) $z_0 = 60$ mm, (c) $z_0 = 80$ mm, (d) $z_0 = 100$ mm when $D = 120$ mm, $L = 120$ mm.

radius varying with the look angle for different edge slopes S_e, the distances z_0, and the fineness ratios.

The fineness ratios of Figs. 13 and 14 are 1 and 1.5, respectively. The figures illustrate that the absolute value of the difference of curvature radius increases with the growing of the look angle. The absolute value of the difference of curvature radius also augments with the growing of the edge slope and the distance z_0 for the same fineness ratio of the conformal dome. It is predicted by the reason that the larger value of z_0 corresponds to the wide range of the dome for the same look angle. Therefore, to reduce the difference of curvature radius, we should make the location of the rotational center nearly the vertex of the dome as far as possible under the construction permitting. Comparing Figs. 13 and 14, we can know that in different fineness ratios, the absolute value of the difference of curvature radius has larger value for the dome with a bigger fineness ratio.

The plot of the angle difference varying with the look angle for different edge slopes S_e, the distance z_0, and the fineness ratios are shown in Figs. 15 and 16. The fineness ratios of Figs. 15 and 16 are 1 and 1.5, respectively. The figures indicate that the angle difference increases at first then decreases with the augment of the look angle. The max value of the angle difference becomes larger with the increasing of the edge slope S_e, and the corresponding look angle is reduced. In addition, the position of the rotational center has weak impact on the angle difference for the same fineness ratio. Comparing Figs. 15 and 16, it can be seen that the angle difference has larger value for the dome with a bigger fineness ratio.

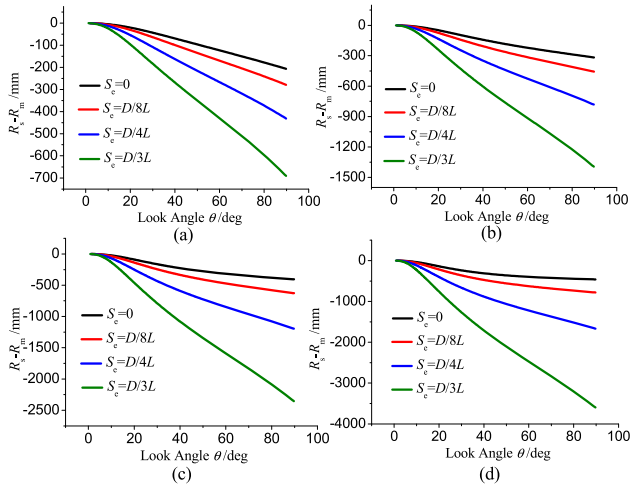

Fig. 14. Difference of curvature radius varying with the look angle for different edge slopes S_e with (a) $z_0 = 60$ mm, (b) $z_0 = 90$ mm, (c) $z_0 = 120$ mm, (d) $z_0 = 150$ mm when $D = 120$ mm, $L = 180$ mm.

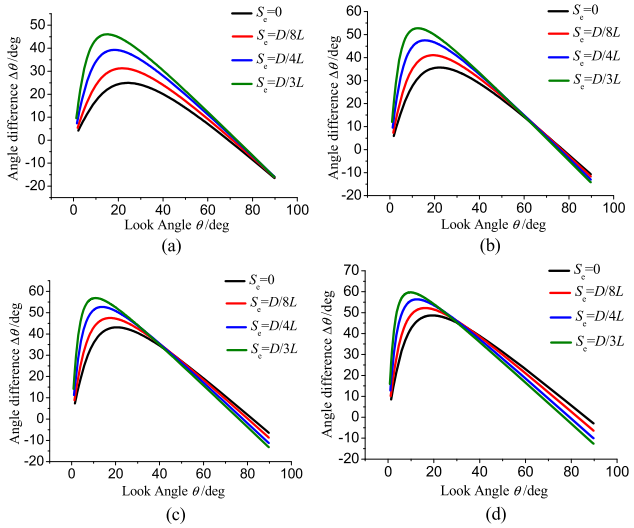

Fig. 16. Angle difference varying with the look angle for different edge slopes S_e with (a) $z_0 = 60$ mm, (b) $z_0 = 90$ mm, (c) $z_0 = 120$ mm, (d) $z_0 = 150$ mm when $D = 120$ mm, $L = 180$ mm.

4. ZERNIKE ABERRATIONS OF CONICOIDAL CONFORMAL DOMES

The wave aberration is a method used to describe the aberrations of optical systems, and it is defined as the optical path difference between the ideal wavefront and the real wavefront. Through expanding the wave aberration function $W(\rho, \phi)$ in terms of a complete set of Zernike polynomials, which are orthogonal over a unit circle, we can get the coefficients of Zernike polynomials [12]. Every term of Zernike polynomials has explicit physical meaning, so the coefficients of Zernike polynomials reflect the value of corresponding aberrations [13,14]. There are two common numbering schemes, the standard Zernike polynomials and the fringe Zernike polynomials. The fringe Zernike polynomials have a maximum of 37 terms, which are a subset of the standard Zernike polynomials but arrange in a different order [15]. The first nine terms of the fringe Zernike polynomials and their corresponding aberrations are shown in Table 2.

Because the optical dome is not a complete optical system, we join a perfect lens in the optical design software CODE V. The perfect lens allows us to investigate dome characteristics without having to discuss properties of imaging systems [12]. Parameters of the model established are shown in Table 3. The dome has the same thickness in the top and bottom, and the inner and outer surfaces have the same edge slope. Previous research indicates the main aberrations of conformal domes are defocus, astigmatism, and coma. Therefore, we will systematically study the Zernike polynomials coefficients of Z4, Z5, and Z8, which represent defocus, astigmatism, and coma, respectively.

Table 2. Zernike Aberration Polynomial

Term	Zernike Polynomial	Aberration Type
Z1	1	Piston
Z2	$\rho\cos(\phi)$	Distortion-Tilt (y-axis)
Z3	$\rho\sin(\phi)$	Distortion-Tilt (x-axis)
Z4	$2\rho^2 - 1$	Defocus-Field curvature
Z5	$\rho^2\cos(2\phi)$	Astigmatism, Primary (axis at 0° or 90°)
Z6	$\rho^2\sin(2\phi)$	Astigmatism, Primary (axis at ±45°)
Z7	$(3\rho^3 - 2\rho)\cos(\phi)$	Coma, Primary (x-axis)
Z8	$(3\rho^3 - 2\rho)\sin(\phi)$	Coma, Primary (y-axis)
Z9	$6\rho^4 - 6\rho^2 + 1$	Spherical Aberration, Primary

Table 3. Parameters of the Model Established

Parameters of Model	Design Value
Materials of the dome	ZnS
Wavelength	4 μm
Thickness of the dome	3 mm
Bottom diameter D	120 mm
Length of the dome L	120 mm, 180 mm
Edge slope S_e	0, $D/8L$, $D/4L$, $D/3L$
Field of regard (FOR)	±50°
Entrance pupil diameter D_0	30 mm
Focal length f'	60 mm

A. Aberration of Defocus (Z4)

The Zernike polynomial coefficient of Z4 represents defocus, and it reflects the size of defocus. Figures 17 and 18 are plots of the coefficient of Z4 for different edge slopes with the rotational center of imaging systems locating different positions when the fineness ratio equals 1 and 1.5.

The figures show that the Zernike polynomial coefficient of Z4 decreases to the minimum value first then increases, and the minimum value gets smaller for the domes with larger edge slopes. This indicates that the changing range of defocus will increase with the growing of edge slopes. Meanwhile, the position of the rotational center has little effect of the minimum

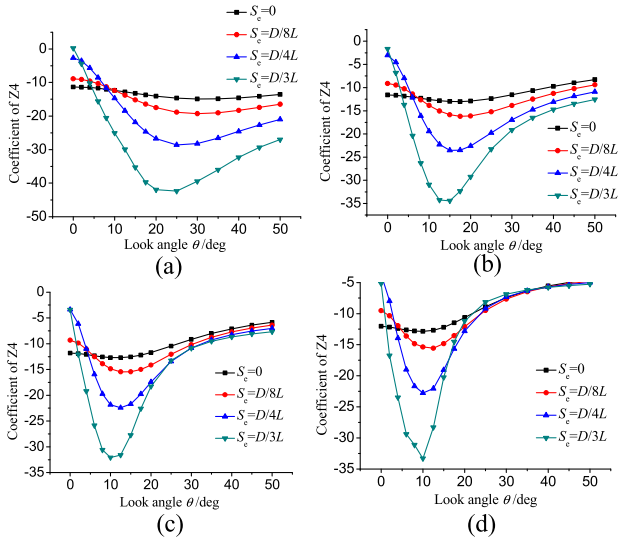

Fig. 17. Coefficient of Z4 for different edge slopes S_e with (a) $z_0 = 40$ mm, (b) $z_0 = 60$ mm, (c) $z_0 = 80$ mm, (d) $z_0 = 100$ mm when $D = 120$ mm, $L = 120$ mm.

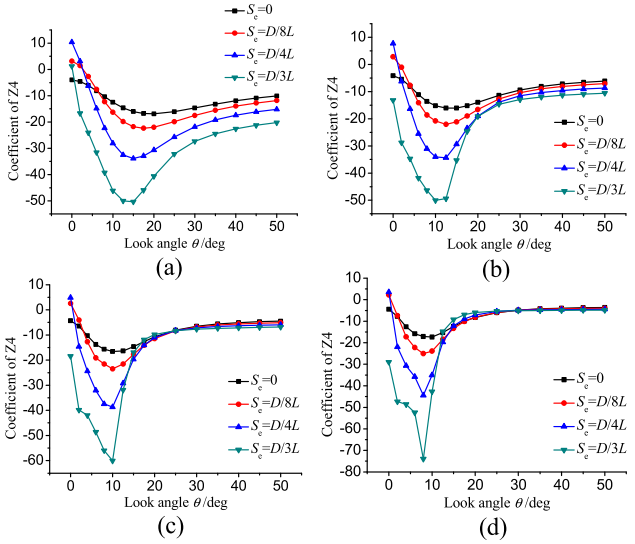

Fig. 18. Coefficient of Z4 for different edge slopes S_e with (a) $z_0 = 60$ mm, (b) $z_0 = 90$ mm, (c) $z_0 = 120$ mm, (d) $z_0 = 180$ mm when $D = 120$ mm, $L = 180$ mm.

value, but it affects the look angle corresponding to the minimum value. The look angle corresponding to the minimum diminishes with the rotational center far away from the vertex of the dome and this causes the changing of defocus rapidly. Comparing Fig. 17 with Fig. 18, it can be seen that the changing range of defocus augments for the dome with a bigger fineness ratio. Therefore, the edge slope and the fineness ratio mainly affect the value of defocus, while the position of rotational centers will impact the changing rate of defocus.

B. Aberration of Astigmatism (Z5)

The Zernike polynomial coefficient of Z5 represents astigmatism, which is mainly affected by the large differences curvatures in the meridian plane and sagittal plane [5]. Figures 19 and 20 are plots of the coefficient of Z5 for different edge slopes with the rotational center of imaging systems locating different positions when the fineness ratio equals 1 and 1.5.

The curves of astigmatism have an intersection point with the line of Z5 = 0, and the intersection point can be seen as a turning point. The curves of astigmatism are divided into two sections. In the first stage, where the look angle changes from zero to the turning point, the coefficient of Z5 increases at first and then descends to zero. In the second stage, where the look angle changes after the turning point, the coefficient of Z5 almost diminishes with the growing of the look angle. The figures show that the coefficient of Z5 has a larger maximum value in the first stage and a smaller minimum value in the second stage for the dome with larger edge slopes. This means the dynamic aberration of astigmatism introduced by the dome increases with the growing of edge slopes. Meanwhile, the positions of rotational centers have little effect on the extreme value of the coefficient of Z5. But the turning point appears in the lower look angle when the rotational center is far away from the vertex of the dome. Comparing Fig. 19 with Fig. 20, it can be seen that the increasing of fineness ratios will aggravate the dynamic aberration of astigmatism. By the reason that astigmatism is mainly affected by the large differences curvatures, we

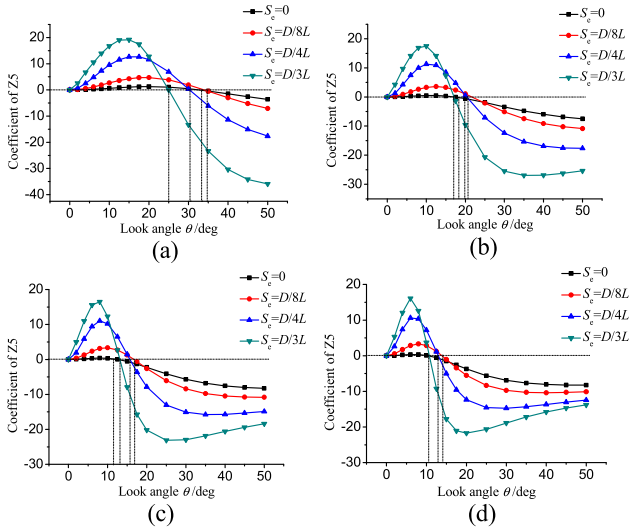

Fig. 19. Coefficient of Z5 for different edge slopes S_e with (a) $z_0 = 40$ mm, (b) $z_0 = 60$ mm, (c) $z_0 = 80$ mm, (d) $z_0 = 100$ mm when $D = 120$ mm, $L = 120$ mm.

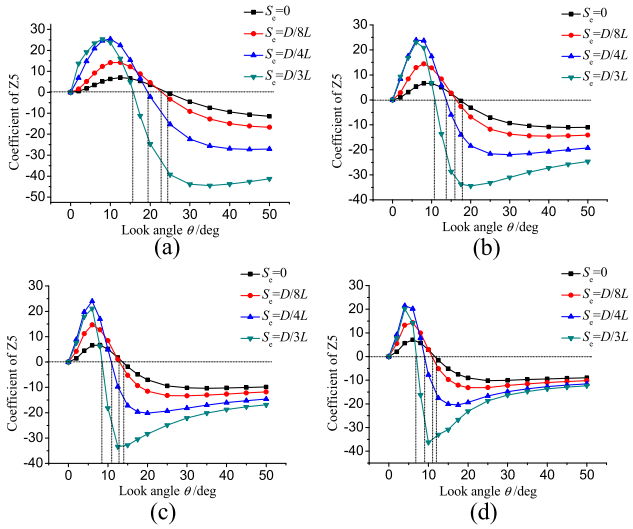

Fig. 20. Coefficient of Z5 for different edge slopes S_e with (a) $z_0 = 60$ mm, (b) $z_0 = 90$ mm, (c) $z_0 = 120$ mm, (d) $z_0 = 180$ mm when $D = 120$ mm, $L = 180$ mm.

will compare Figs. 19 and 20 with Figs. 13 and 14 in the following. The plots of these figures are obtained in the same condition. In Figs. 13 and 14, the curves decline with the growing of the look angle. This is similar with the curves in the second stage of Figs. 19 and 20. The difference is Figs. 19 and 20 exist the first stage in which the aberration of astigmatism changes sharply. It is not unexpected by the reason that the aberration of astigmatism gets from a imaging system with the entrance pupil diameter of 30 mm while the difference of curvature radius gets from a point on the surface. When the scanning angle of imaging systems changes nearby 0°, the symmetry of the conformal dome participating in imaging comes about significant variations.

C. Aberration of Coma (Z8)

The Zernike polynomial coefficient of Z8 represents coma, which is mainly affected by the angle between the axis of the imaging system and the surface normal [5]. Figures 21 and 22 are plots of the coefficient of Z8. Similar to the curves of astigmatism, the curves of coma also have an intersection point with the line of Z8 = 0. The curves of coma are divided into two sections by the turning point. Different from the curves of Z5, in the first stage, the coefficient of Z8 descends at first and then increases to zero. While in the second stage, the coefficient of Z8 increases at first and then diminishes with the growing of the look angle. The figures show that the dynamic aberration of coma introduced by the dome increases with the growing of the edge slopes. Meanwhile, the positions of rotational centers also have little effect on the extreme value of the coefficient of Z8 but affect the position of the turning point. Comparing Fig. 21 with Fig. 22, it can be seen that the increasing of fineness ratios will aggravate the dynamic aberration of coma. Comparing with Figs. 15 and 16, which are the plots of the angle between the axis of the imaging system and the surface normal, the curves of Z8 in the second stage of Figs. 21 and 22 have similar rules with the plots in Figs. 15 and 16.

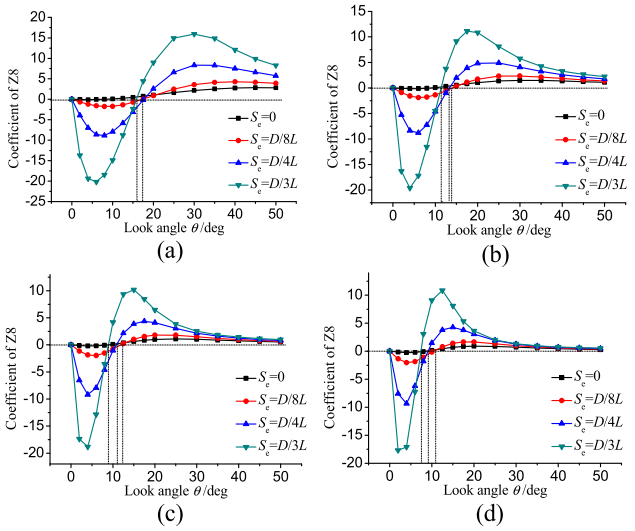

Fig. 21. Coefficient of Z8 for different edge slopes S_e with (a) $z_0 = 40$ mm, (b) $z_0 = 60$ mm, (c) $z_0 = 80$ mm, (d) $z_0 = 100$ mm when $D = 120$ mm, $L = 120$ mm.

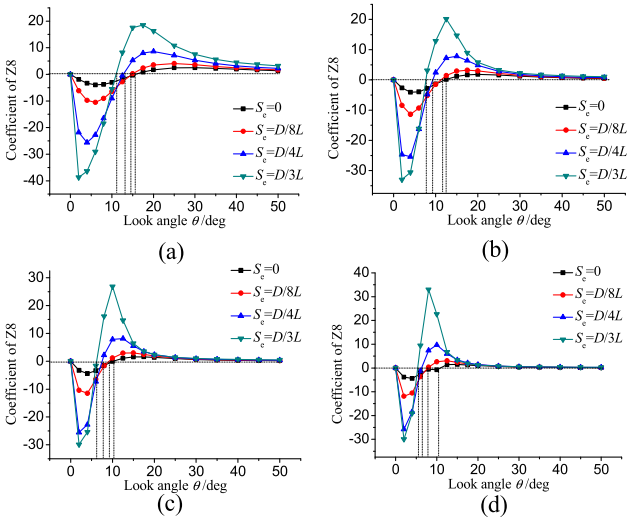

Fig. 22. Coefficient of Z8 for different edge slopes S_e with (a) $z_0 = 60$ mm, (b) $z_0 = 90$ mm, (c) $z_0 = 120$ mm, (d) $z_0 = 180$ mm when $D = 120$ mm, $L = 180$ mm.

Figures 21 and 22 also have a stage in which the aberration of coma changes rapidly. As analyzed before, it is caused by the significant variations of symmetry of the conformal dome participating in imaging.

5. CONCLUSION

This paper investigated the geometric characteristics of quadric surfaces and the Zernike aberrations of conicoidal conformal domes. As indicated by previous researchers, for a quadric surface with decided bottom diameter and length, the edge slope determines the surface type (ellipsoid, paraboloid, or hyperboloid). Based on this, this paper first proved that the Dupin index line of a quadric surface is an ellipsoid and the radius of curvature has extreme values in the meridian plane and sagittal plane. Then the uniform formulas of curvature that were suitable for ellipsoid, paraboloid, and hyperboloid were deduced. The Zernike aberrations of defocus, astigmatism, and coma for the dome with different edge slopes, fineness ratios, and positions of the rotational centers are analyzed systematically. The research indicates that the dynamic ranges of defocus, astigmatism, and coma increase with the growing of edge slopes and fineness ratios, but have little change with the variation of the rotational center positions. The positions of rotational centers mainly impact the changing rate of defocus. The curves of Z5 and Z8 have turning points, the positions of which are mainly affected by the positions of rotational centers. The turning points divide the curves into two sections. In the first section, the curves change rapidly. It is by the reason that the symmetry of the conformal dome participating in imaging comes about significant variations. While in the second section, the curves change smoothly. Comparing with the curves of curvature differences and the angle between the axis of the imaging system and the surface normal, the curves in the second sections of Z5 and Z8 are similar to them, respectively. These verify astigmatism is affected mainly by the curvature difference and the angle difference mainly affects coma. In addition, due to the existence of first sections, the interval of scanning angles should be smaller in the lower scanning angle when designing the conformal systems.

REFERENCES

1. P. A. Trotta, "Precision conformal optics technology program," Proc. SPIE **4375**, 96–107 (2001).
2. P. M. James, "Conformal optics: theory and practice," Proc. SPIE **4442**, 101–107 (2001).
3. A. B. Shorey, W. Kordonski, J. Tracy, and M. Tricard, "Developments in the finishing of domes and conformal optics," Proc. SPIE **6545**, 65450Q (2007).
4. D. J. Knapp, "Conformal optical design," Ph.D. dissertation (University of Arizona, 2002).
5. K. S. Ellis, "The optics of ellipsoidal domes," Ph.D. dissertation (University of Arizona, 1999).
6. G. C. Blake, B. M. Dean, and P. M. James, "Aberrations of optical domes," Proc. SPIE **3482**, 48–61 (1998).
7. J. E. Pond, C. T. Welch, and G. W. Sutton, "Side-mounted IR window aero-optic and aerothermal analysis," Proc. SPIE **3705**, 180–188 (1999).
8. L. R. Thomas Davenport, "3D NURBS representation of surfaces for illumination," Proc. SPIE **4832**, 293–301 (2002).
9. S. M. Kamali, A. Arbabi, F. Arbabi, E. Arbabi, Y. Horie, and A. Faraon, "Decoupling optical function and geometrical form using conformal flexible dielectric metasurfaces," Nat. Commun. **7**, 11618 (2016).
10. L. Li, Y. Li, Y. F. Huang, and B. L. Du, "The research of conformal optical design," Proc. SPIE **7383**, 73833M (2009).
11. D. J. Knapp, "Fundamentals of conformal dome design," Proc. SPIE **4832**, 394–409 (2002).
12. J. Y. Wang and D. E. Silva, "Wave-front interpretation with Zernike polynomials," Appl. Opt. **19**, 1510–1518 (1980).
13. Y. M. Liu, J. Ma, H. P. Ma, and X. Z. Jiang, "Zernike aberration characteristics of precision conformal optical windows," Proc. SPIE **7544**, 75443W (2010).
14. W. Zhang, B. J. Zuo, S. Q. Chen, H. S. Xiao, and Z. G. Fan, "Design of fixed correctors used in conformal optical system based on diffractive optical elements," Appl. Opt. **52**, 461–466 (2013).
15. CODE V Reference Manual, ORA (Optical Research Associates).